



Article

# Metal-Porphyrin-Based Covalent Organic Framework Composite Membrane for Salts and Dyes Separation

Fatimah Al-Ghazzawi <sup>1,\*</sup>, Mohammed Mahdi Al-Mossawi <sup>2</sup> and Hadeel K. Allayeith <sup>3</sup>

- <sup>1</sup> Al-Nasiriyah Technical Institute, Southern Technical University, Thi-Qar, Nasiriyah 64001, Iraq
- Marine Geology Department, Marine Science Center, University of Basrah, Basrah 61004, Iraq; mohammed.mahdi@uobasrah.edu.iq
- Department of Chemistry, Collage of Science, University of Basrah, Basrah 61004, Iraq; hadeel.kadhum@uobasrah.edu.iq
- \* Correspondence: fanag83@stu.edu.iq

#### **Abstract**

Covalent organic framework (COF) membranes are eminent candidates in filtration and separation applications due to their high porosity, ordered pore size, versatile molecular structure, inherent mechanical properties, and excellent stability. However, large-scale COF membranes suffer from several issues, including stacking and crystal defects, which negatively impact their rejection performance. In this study, a continuous thin film of porphyrinic-based COF (i.e., COF-TCPP (Fe)) with various thicknesses was fabricated on a PVDF support layer via a vacuum-assisted interfacial polymerization method. The composite membranes were then characterized, and their filtration and dye/salt separation performance were evaluated using a dead-end filtration cell. The results showed that the rejection efficiencies of Congo red and acid fuchsin for the optimal proposed membrane were 99.5% and 95.8%, respectively. In comparison, the corresponding values for the pristine membrane were 73.3% and 62.8%. The results also showed that with an increase in the COF loading concentration during synthesis, the membrane flux decreased, while the rejection efficiency increased. This study proposes a simple and effective method to mitigate the large-scale issues of COF-based membranes and to enhance the separation performance of existing polymeric membranes.

**Keywords:** covalent organic frameworks; vacuum-assisted interfacial polymerization; dye separation; nanofiltration; composite membrane



Academic Editor: Valentina Gargiulo

Received: 8 July 2025 Revised: 9 August 2025 Accepted: 26 August 2025 Published: 28 August 2025

Citation: Al-Ghazzawi, F.; Al-Mossawi, M.M.; Allayeith, H.K. Metal–Porphyrin-Based Covalent Organic Framework Composite Membrane for Salts and Dyes Separation. *Compounds* 2025, 5, 34. https://doi.org/10.3390/ compounds5030034

Copyright: © 2025 by the authors. Licensee MDPI, Basel, Switzerland. This article is an open access article distributed under the terms and conditions of the Creative Commons Attribution (CC BY) license (https://creativecommons.org/licenses/by/4.0/).

#### 1. Introduction

Despite water covering up to 71% of the Earth's volume, accessing freshwater for daily use remains challenging [1]. The shortage of freshwater resources has become a significant concern over the last two decades, primarily due to the issue of overpopulation, particularly in developing countries where water resources are contaminated with various chemicals [2,3]. On the other hand, various commercial and industrial sources discharge wastewater into the living environment. The wastewater typically contains a diverse range of hazardous pollutants, including inorganic salts, dyes, heavy metals, pharmaceuticals, and other impurities [4,5]. It was stated that approximately 700,000 tons of dyes are produced annually worldwide for various applications [6], with 60% of these used in the dyeing process and textile factories [7]. The discharged wastewater from the textile factories is usually high in salt and dye concentrations [8]. These chemicals can cause serious harm

Compounds **2025**, 5, 34 2 of 20

to the environment. Therefore, it is of great importance to develop an effective method for separating salt and dye.

Various separation methods have been developed, including advanced oxidation, photocatalysis, adsorption, biological, and membrane separation methods [9]. However, these methods are limited in their use due to low removal efficiency, high cost, long processing times, and high dependence on specific conditions [10]. Among all the membrane separation technologies, nano-filtration (NF) membranes, which consist of polymeric porous substrate and dense selective layer, are considered to be effective and a promising method as they can offer high water flux and rejection efficiency for multivalent ions and dyes with a molecular weight cut-off (MWCO) varying from 100 to 1000 Da as well as operate at low pressure [8]. However, commercially available NF membranes achieve high rejection for both salts and dyes. Accordingly, the loose nano-filtration (LNF) membrane has been introduced to satisfy this limitation as the selective layer of LNF is designed to yield high dye rejection efficiency but low salt rejection efficiency [11]. LNF membranes are widely used in dye production processes to enhance the quality of the dye and improve dye recovery ability, as salts are added during dye synthesis [12].

Over the last few years, various porous materials have been utilized as selective layers in LNF membranes to achieve high water flux and efficient rejection. Metal-organic frameworks (MOFs) were considered a suitable choice due to their porous structure [13–15]. However, a series of studies has revealed that MOFs are susceptible to degradation by water [16–18] and exhibit low resistance to environmental conditions [19–21].

To overcome these limitations, covalent organic frameworks (COFs) have been proposed as a selective layer in LNF membranes used in filtration, separation, and water desalination applications [22,23]. COFs possess high porosity, ordered pore size, a versatile molecular structure, inherent mechanical properties, and excellent stability [1]. Several COFbased membranes have demonstrated competitive performance in dye separation [24–36]. COFs demonstrate a high potential in fabricating nanofiltration membranes. However, they are usually synthesized in the form of an insoluble powder, and hence it is not easy to form them as a large-scale membrane [37]. This is due to the higher crystallinity of the COF powder compared to that of the COF membrane [38]. Therefore, the reported COF membranes suffered from crystal and stacking issues, which affected the separation performance and the mechanical properties of the membranes [38]. Kong et al. [39] attempted to fabricate a defect-free COF membrane by using trimesoyl chloride (TMC) to stitch the defects among the COF crystals and cross-link the COF cavities, resulting in a high degree of cross-linking network. The resulting membrane exhibited a water permeability of  $0.81~{\rm L~m^{-2}~h^{-1}}$  bar  $^{\rm l}$  and achieved a significant enhancement in NaCl rejection, increasing from almost negligible to 93.3% at 5 bar. Additionally, a continuous, selective layer of COF was formed on the substrate. Zhang et al. [40] fabricated a COF-TATP/nylon membrane that had an exceptional dye rejection (100%) against Congo red (CR). They used CR to stitch the defects in the COF layer through a chemical procedure. The results showed that the presence of CR in the solution of other dyes could improve their rejection efficiency.

On the other hand, the COF layers tend to aggregate owing to the strong interactions of the interlayer dipole [41]. This can affect the fabrication of ultrathin membranes, which negatively influence the permeability of the membrane during the separation process. Among the various methods attempted to prevent the aggregation issue, introducing macrocycles into the COF system can be considered an ideal solution [42].

Porphyrin is a typical planar and rigid macrocycle featuring low rotational freedom, which can produce crystalline structures to build COFs and MOFs networks [43]. The porphyrin served as the main backbone and directly contributed to the building of the frameworks of COFs/MOFs [44]. A few porphyrinic-based MOF membranes have been

Compounds 2025, 5, 34 3 of 20

reported in the literature for nanofiltration and dye separation applications. For instance, Hussain and Peng [45] synthesized Fe-TCPP MOF nanofibers and applied them as a selective layer of thin-film nanocomposite membrane for nanofiltration. The resulting membrane featured a continuous interlayer and yielded an enhanced water flux of 3.5 times compared to the membrane without the selective layer. Additionally, the membrane exhibited high rejection efficiency against the dyes and demonstrated good antifouling characteristics.

From the above, it can be concluded that the presence of the porphyrin in the COF framework can produce a free-defect interlayer in composite nanofiltration membranes and improve their permeability and selectivity performance. However, it seems that using a porphyrin-based COF/polymeric composite membrane in the application of dyes/salts separation and filtration has not been reported. Therefore, a porphyrinic-based COF nanocomposite membrane was fabricated and tested for nanofiltration and separation of salts and dyes. COF-TCPP (Fe) was first synthesized and then deposited onto PVDF porous membranes (0.22  $\mu m$ ) using the vacuum-assisted interfacial polymerization method. Various salts and dyes (i.e., NaCl, Na2SO4, MgCl2, CaCl2, MgSO4, Congo red, and acid fuchsin) were used to evaluate the performance of the fabricated membrane. Furthermore, the proposed membrane was produced at different concentrations of COF-TCPP (Fe) to quantify the effect of COF loading on the membrane's performance.

# 2. Materials and Methods

#### 2.1. Materials

Flat sheets of PVDF membrane with a pore size of 0.22  $\mu m$  and a thickness of 100  $\mu m$  were purchased from Tianshan Precision Filter Material Co., Ltd. (Hangzhou, China). The moisture diffusivity of the pristine membrane used in this study was measured in a previous study to be approximately  $1.62 \times 10^{-6}$  m<sup>2</sup>/s [46], indicating good water permeability and justifying its selection. All the other chemicals, including COF regents, dyes, salts, and solutions, were purchased from Sigma-Aldrich (Chengdu, China) and used without purification.

# 2.2. Synthesis of TMCPP (5,10,15,20-Tetrakis (4-Methoxycorbonyl Phenyl) Porphyrinate)

Methyl 4-formylbenzoate (0.1 mol, 16 g) was dissolved in 350 mL of propionic acid and refluxed at  $140\,^{\circ}$ C, and distilled pyrrole (10 mL) in 15 mL of propionic acid was added dropwise over 30 min. The mixture was stirred and refluxed together for approximately 1 h. After that, the mixture solution was cooled to room temperature and filtered under vacuum and washed with MeOH. Purple crystals of TMCPP were collected and dried [47].

# 2.3. Synthesis of TMCPP (5,10,15,20–Tetrakis (4-Methoxycorbonyl Phenyl) Porphyrinate) with Fe (II)

TMCPP (1 g, 0.01 mol) was dissolved with 2 qu. of Iron (II) chloride tetra hydrate in 200 mL of DMF. The mixture was refluxed together at 150  $^{\circ}$ C for about 6 h under N<sub>2</sub> gas. The reaction was then exposed to air overnight. The solution was filtered under vacuum and washed twice with water. The yield was dried in an oven to obtain a brown powder of TMCPP Fe(III) [48].

# 2.4. Synthesis of TCPP (Fe (III))

TMCPP(Fe) (1 g, 0.001 mol) was dissolved with 1 M of KOH in 50 mL THF and 50 mL MeOH, and then refluxed at 66  $^{\circ}$ C for about 72 h. We added 1 M of HCl and water to the solution. The solution was filtered under vacuum and washed twice with water. The yield of the TCPP (Fe(III)) synthesis was dried overnight in an oven [48]. The synthesis steps of the TCPP(Fe) ligand are shown in Figure 1.

Compounds 2025, 5, 34 4 of 20

**Figure 1.** Synthesis steps of TCPP(Fe).

#### 2.5. Synthesis of COF-TCPP (Fe)

TCPP(Fe) (88.6 g, 0.1 mol) was dissolved with Benzenediamine (22 g, 0.2 mol) in 40 mL of THF. The solution was added to a mixture of solvent N,N-Diisopropylethylamine (DIPEA) as the base and N,N'-dicyclohexylcarbodiimide (DCC) as the catalyst. The mixture was stirred on a magnetic stirrer in a Pyrex tube. The Pyrex tube was placed in an oven at 120  $^{\circ}$ C for approximately 72 h. Then, the solution was filtered under vacuum and washed twice with EtOH. The yield was dried in an oven overnight [49,50]. Figure 2 shows the chemical structure of COF-TCPP (Fe).

#### 2.6. Membrane Pre-Treatment

Firstly, the membrane samples were treated in the chamber of the plasma cleaner ( $O_2$ ) at a temperature of 25 °C for 10 min. The membrane samples were then treated using APTES. The samples were soaked in an APTES-toluene solution of 2% (v/v) for 1 day under  $N_2$ . Later, the samples were washed three times with acetone/ethanol and dried.

#### 2.7. Preparing COF-TCPP (Fe)@ PVDF Membrane

The vacuum-assisted interfacial polymerization method was used in this study to fabricate the modified membrane, which can be considered a scalable method [51]. It can produce a composite membrane within a large area based on the inner diameter of the vacuum cell. Furthermore, the method does not require a heating device, thereby it can be used in laboratories to fabricate large-scale membranes. The preparation of COF-TCPP (Fe)@ PVDF membranes is described in Figure 3. Firstly, the PVDF membrane is treated as explained above. After treating the surface of the membrane and enhancing the interaction between the COF-TCPP(Fe) and PVDF membrane, the stable suspension of COF-TCPP (Fe) was prepared by dispersing the powder in DI water under ultrasonication for 2 h. After that, the mixture was filtered on the treated PVDF membrane under a vacuum pressure of

Compounds **2025**, 5, 34 5 of 20

80 kPa. The filtration mixture was prepared at various COF concentrations, including 4, 8, 12, and 16 mg mL<sup>-1</sup>, and the corresponding resultant membranes were represented as M1, M2, M3, and M4, respectively, while M0 represented the pristine PVDF membrane. In this study, the inner diameter of the dead-end cell was 5 cm; thereby, the area of COF-TCPP (Fe) was  $19.6 \text{ cm}^2$ . Figure 4 shows the digital photos of the resultant membranes. The photos demonstrated a uniform distribution of COF-TCPP (Fe) particles on the surface of the substrate without any defects or cracks. The presence of the NH<sub>2</sub> group on the surface of the treated substrate assisted the COF particles in creating chemical bonds with the surface and attaching firmly to the substrate.

Figure 2. Chemical structure of COF-TCPP (Fe).

Compounds **2025**, 5, 34 6 of 20

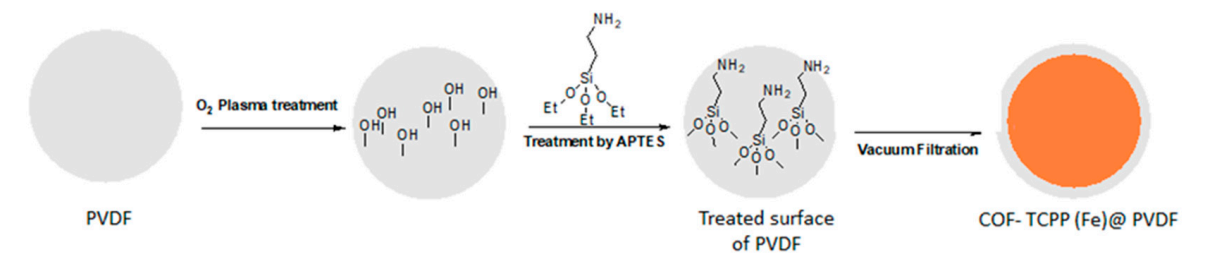


Figure 3. Schematic representation of COF-TCPP (Fe)@ PVDF membrane preparation.

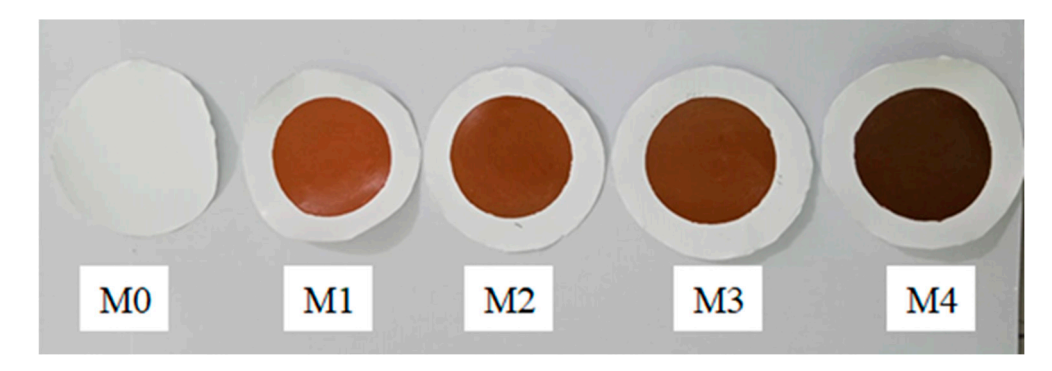


Figure 4. The resultant COF-TCPP (Fe)@ PVDF membranes at different COF concentrations.

#### 2.8. COFs and Membranes Characterization

The surface function of the membranes (hydrophobicity/hydrophilicity) was examined through the water contact angle (WCA) by using a goniometer ( $\pm 3^{\circ}$ ). The membrane surface charge was quantified by measuring the Zeta potential using a SurPASS electrokinetic analyzer (Anton Paar compony, Graz, Austria). Potassium chloride (KCl) with a concentration of 0.01 M was used as an electrolyte solution. The morphology of the pristine and modified membranes was revealed using scanning electron microscopy (FE-SEM, JEOL-JSM 6490 AF, JEOL Ltd.—Japan Electron Optics Laboratory, Tokyo, Japan) at an accelerating voltage of 15 kV. The X-ray diffraction patterns (XRD) of the COF, pristine, and modified membranes were examined using a GBC-MMA X-ray diffractometer (GBC Scientific Equipment Pty Ltd, Victoria, Australia) with a diffraction angle (2θ) ranging from 5 to  $40^{\circ}.$  TGA-DSC was conducted using NETZSCH STA 449F Jupiter simultaneous analyzer (NETZSCH-Gerätebau GmbH, Selb, Germany), which was connected to a multichannel temperature controller (TR004). The samples were heated from 25 to 500 °C with a heating rate of 10 °C/min under a  $N_2/O_2$  atmosphere, with a flow rate of 20 cm<sup>3</sup>/min. The thickness of the deposited layers of COF was measured using a Veeco dektak 150 Stylus profilometer (Veeco Instruments Inc, Plainview, New York, NY, USA). The thickness of each sample was recorded at four positions and then averaged. The Fourier transform infrared spectra (FTIR) test was conducted using a Nicolet iS5 instrument (Thermo Fisher Scientific, Waltham, MA, USA). The samples were scanned in the range of 4000 to 600 cm<sup>-1</sup>. The gas adsorption test was performed for the COF-TCPP (Fe) powder using the Quantachrome Autosorb MP device (Quantachrome Instruments Inc., Boynton Beach, FL, USA). We implemented 99.99% pure N<sub>2</sub> in the tests. The surface area was then calculated based on Brunauer-Emmett-Teller (BET). A Shimadzu EZ-S universal test device (Shimadzu Corporation, Kyoto, Japan) was used to perform tensile tests for the examined membranes to estimate the mechanical properties.

### 2.9. Nanofiltration Experiments

The water permeability and the rejection efficiency of the pristine and modified membranes were determined using a dead-end filtration cell with a diameter of 5 cm. To

Compounds **2025**, 5, 34 7 of 20

reach the steady state, each membrane was first pre-pressed at 6 bar for 30 min and then tested at room temperature and a pressure of 5 bar with magnetic stirring. The pure water flux (PWF) was calculated from the following Equation (1) [8]

$$PWF = \frac{V}{S t P}$$
 (1)

where V is the volume of permeate in L, S is the area of the membrane (19.625 cm<sup>2</sup>), t is the time of the test in h, and P is the trans-membrane pressure in bar.

The rejection efficiency (R) of the salts and dyes was calculated from Equation (2) [8]

$$R = \left(1 - \frac{C_p}{C_f}\right) \times 100\% \tag{2}$$

where  $C_p$  (mg/L) and  $C_f$  (mg/L) are the salt/dye concentration at the permeate and feed solution, respectively.

The salt concentration in the permeate/feed solution was determined from the electrical conductivity, while the dye concentration in the permeate, feed, and retentate solutions was measured using the maximum absorption wavelength of the UV absorbance graph.

# 3. Results and Discussion

#### 3.1. Membrane Characterization

The membrane surface morphology was investigated using SEM, and the results are presented in Figure 5. The pristine membrane consisted of enormous fibers with micronsized pores (Figure 5a). The images of M2, M3, and M4 are presented in Figure 5b–d, respectively. It can be observed that there is a uniform deposition of the COF particles on the surface and within the pores of the membrane. The images also show that the surfaces of M2 and M3 were approximately covered with COF particles. However, it was fully covered for the case of M4 due to the increase in the COF concentration. In addition to the SEM micrographs, the thickness of the COF-deposited layers of M2, M3, and M4 was measured and is presented in Figure 6. The measurement was conducted at four random positions on each membrane. It is evident that with an increase in the COF loading, the thickness of the deposited layer also increases. The average thicknesses of M2, M3, and M4 were 0.324, 0.536, and 0.764  $\mu$ m, respectively.

Figure 7a shows the XRD patterns of the COF-TCPP (Fe) powder, pristine membrane, and the modified membrane. It can be seen that the COF powder exhibits diffraction peaks at  $3.5^{\circ}$  (strong) and  $7.2^{\circ}$  (weak) [49]. To explore the structure of COF-TCPP (Fe) and estimate the unit cell parameters, a structural model was built using VESTA software version 3.5.8 (Figure 7b). The distinct wavelength ( $\lambda$ ) of Cu K $\alpha$  radiation was taken as 0.15406 nm [52]. A quasicrystal unit cell with a Lattice parameter of a = 27.5879 Å was proposed, which offered good agreement between the experimental and simulation PXRD patterns of the COF-TCPP (Fe). The presence of hydrogen bonds can efficiently prevent the movement of the molecular chains during the formation of COF and thus mitigate the formation defects and improve the crystallinity [53]. The groups of N-H and O=C in the structure of COF-TCPP (Fe) can bond together to create hydrogen bonds. The presence of the intramolecular hydrogen bond (N-H···O=C) enhances the structural rigidity of COF and subsequently improves the crystallinity.

The pattern of the pristine membrane shows diffraction peaks at  $18.6^{\circ}$ ,  $20.7^{\circ}$ ,  $26.5^{\circ}$ , and  $36.7^{\circ}$ , which agree well with the pattern reported in Ref. [14]. The XRD pattern of the modified membrane shows the clear peaks of COF-TCPP (Fe), indicating a successful deposition of the COF particles on the surface of the membrane.

Compounds **2025**, 5, 34 8 of 20

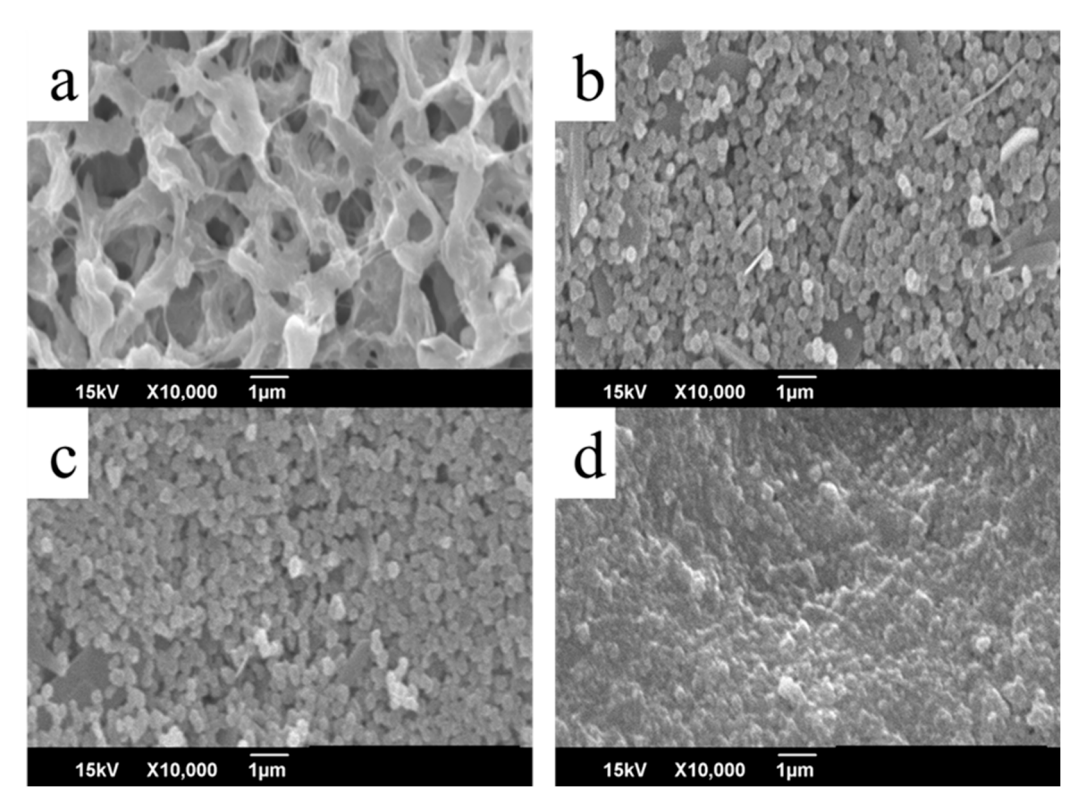


Figure 5. SEM images of surface morphology for (a) M0, (b) M2, (c) M3, and (d) M4.

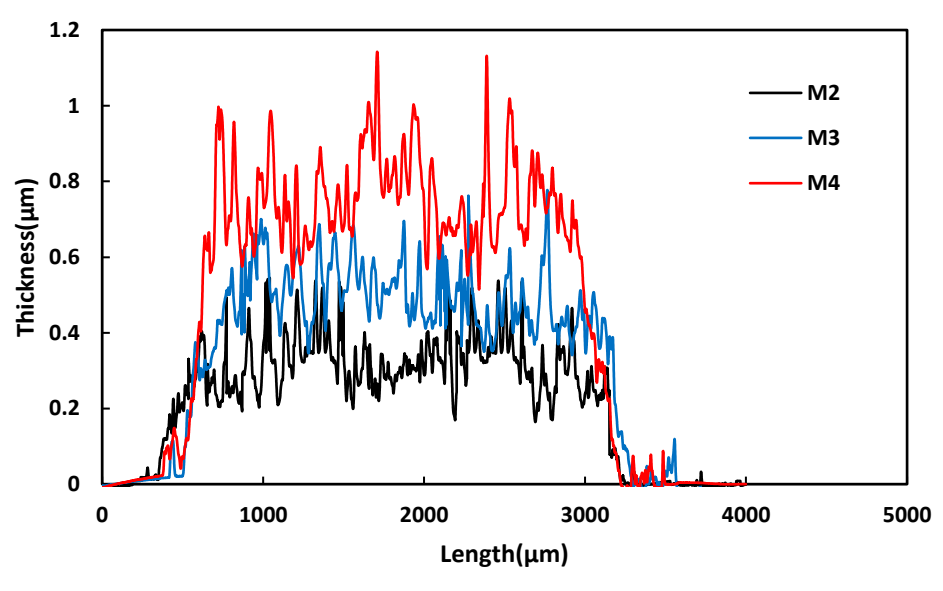
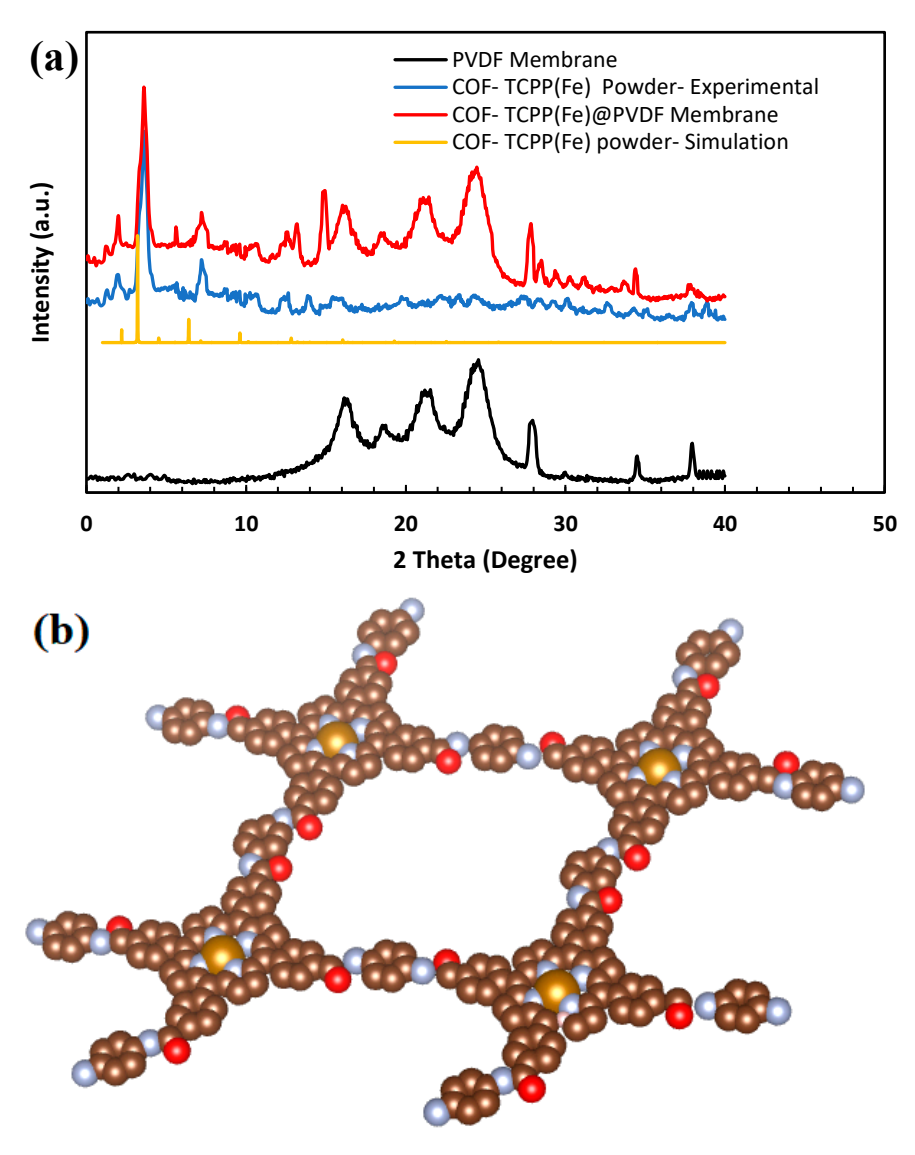


Figure 6. The thickness of the COF deposited layer of M2, M3, and M4.

To confirm the formation of an amide bond between Benzenediamine and COF-TCPP (Fe), an FT-IR test was conducted. As presented in Figure 8, the FT-IR spectrum of TCPP (Fe) exhibited a peak at 800 and 1070 cm<sup>-1</sup> for the porphyrin structure, which includes the CH bond of the benzene and pyrrole rings, and a peak at 3200 cm<sup>-1</sup> of N-H. The vibration absorption peak of the C=N bond appears at 1626 and 1017 cm<sup>-1</sup> for the Fe-N bond [54]. The vibration absorption peaks of the benzene ring appear at 3250, 1725, and 1255 cm<sup>-1</sup>, corresponding to the -OH, C=O, and C-O stretching vibrations in the carboxyl groups, respectively [55,56]. The FT-IR spectrum of COF-TCPP(Fe) indicates the vanishing of the vibration absorption peak of -OH and C-O of carboxyl groups. They appear at about 1740 and 1577 cm<sup>-1</sup>, attributed to the C=O and NH<sub>2</sub> of the O=C-NH, and at 3345 cm<sup>-1</sup>, attributed to the NH of Benzenediamine [57].

Compounds **2025**, 5, 34 9 of 20



**Figure 7.** (a) XRD patterns of the COF-TCPP (Fe) powder (EXP.), COF-TCPP (Fe) (Sim.), pristine membrane, and the modified membrane; (b) space-filling model of COF-TCPP (Fe).

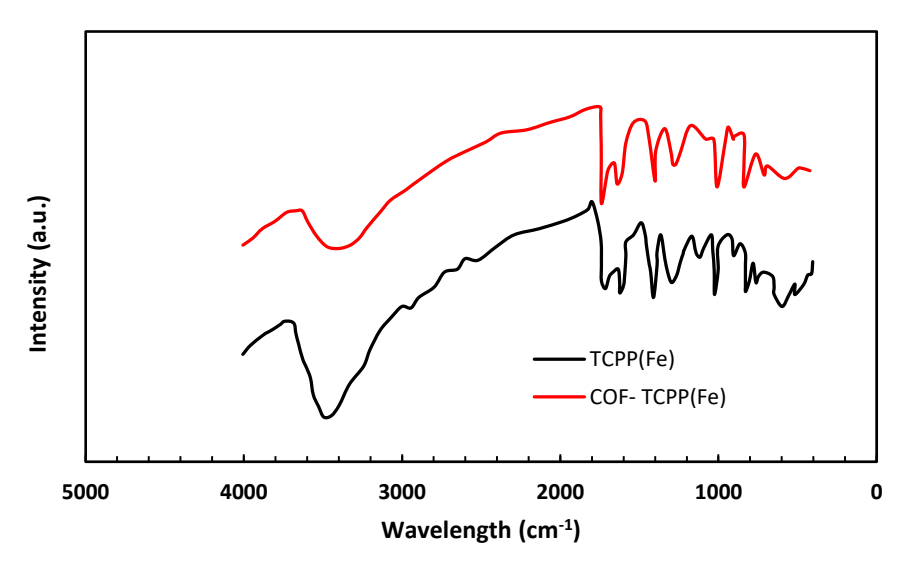
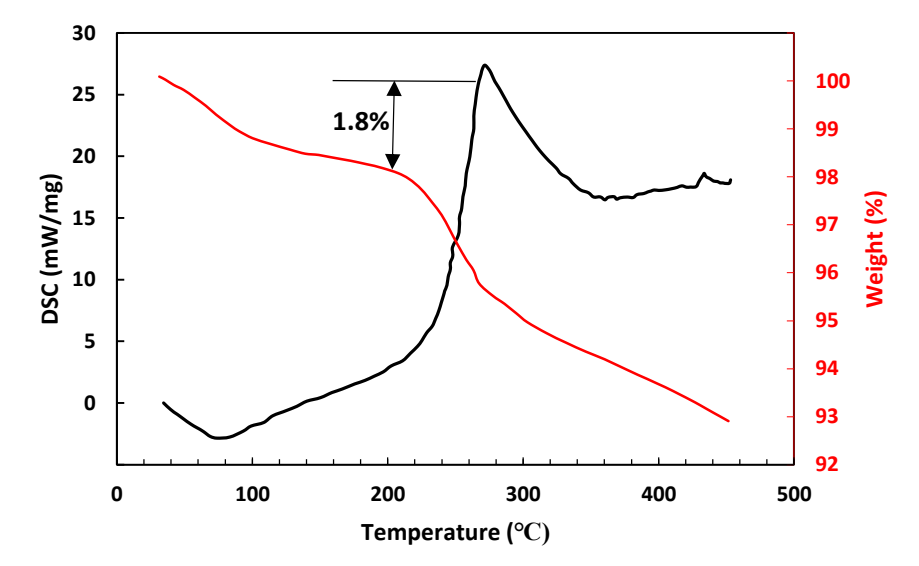


Figure 8. FT-IR spectra of TCPP (Fe) and COF-TCOO (Fe).

The TGA was measured for COF-TCPP(Fe), and the result is illustrated in Figure 9. It can be seen that the sample lost 1.8% of its weight when the temperature increased from

Compounds **2025**, 5, 34 10 of 20

70 °C to 180 °C. This might be due to the loss of the moisture,  $H_2O$ , and solvents. The TGA results of COF-TCPP (Fe) also showed that the sample was stable at 200 °C [57].



**Figure 9.** TGA-DSC curves of COF-TCPP (Fe) at a heating rate of 10 °C/min and  $N_2/O_2$  with a flow rate of 20 cm<sup>3</sup>/min.

Figure 10 shows  $N_2$  adsorption–desorption isotherms and the pore diameter distribution of COF-TCPP (Fe). The adsorption–desorption graphs showed a pattern that agreed well with type-I isotherms, as  $N_2$  uptake increased steeply under low relative pressures, indicating the microporous structure of COF-TCPP (Fe). A small hysteresis loop was associated with the sharp increase in  $N_2$  uptake at higher relative pressures ( $P/P_0 > 0.9$ ), which can be attributed to the presence of a minor fraction of mesopores. The pore distribution supports this finding, as the curve exhibited a narrow and intense peak at approximately 2 nm. After that, the curve gradually extended to the mesoporous region (>2 nm). This behavior indicated a predominantly uniform microporous–small mesoporous framework, with limited mesopores likely responsible for the hysteresis at the higher relative pressures. The behavior was similar to ones reported in previous studies for porphyrin-based COF [58,59]. The specific surface area ( $S_{\rm BET}$ ) and the average pore diameter were estimated as 860.53 m<sup>2</sup>g<sup>-1</sup> and 1.86 nm, respectively.

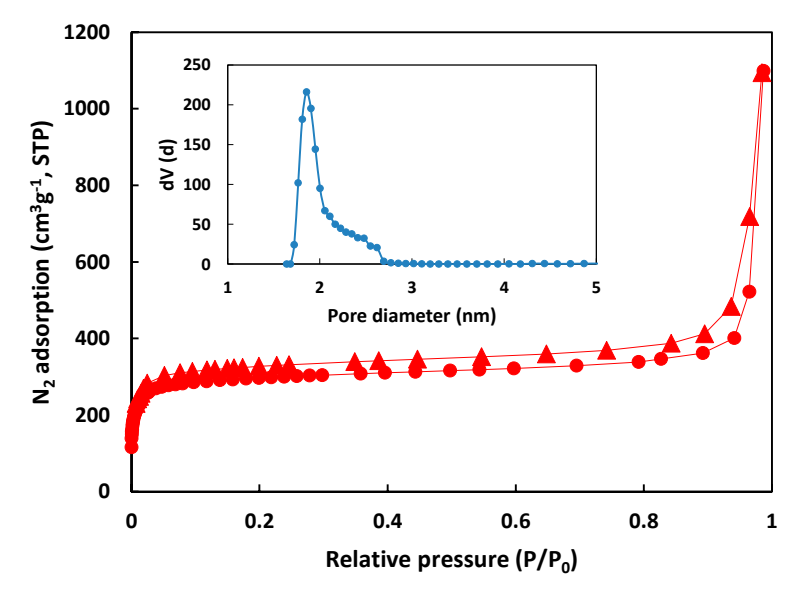


**Figure 10.** Adsorption-desorption and pore size distribution of COF-TCPP (Fe) at  $N_2$  purity of 99.99% and temperature of 77 K.

Compounds **2025**, 5, 34

#### 3.2. Membrane Surface and Mechanical Properties

The surface hydrophilicity and charge of the investigated membranes were examined using static water contact angles and zeta potentials, respectively. Figure 11 shows the water contact angle (WCA) and zeta potential of the various membranes. The pristine PVDF membrane exhibited low hydrophilicity, with a WCA of  $74.3^{\circ} \pm 5.4^{\circ}$ . The deposition of COF-TCPP (Fe) on the membrane surface improved its hydrophilicity, as the WCA of M1 was lower than that of M0 by about  $14^{\circ}$ . However, the further increase in the loading of COF-TCPP (Fe) had almost no effect on the membrane hydrophilicity, as the WCA of M2, M3, and M4 was approximately the same.

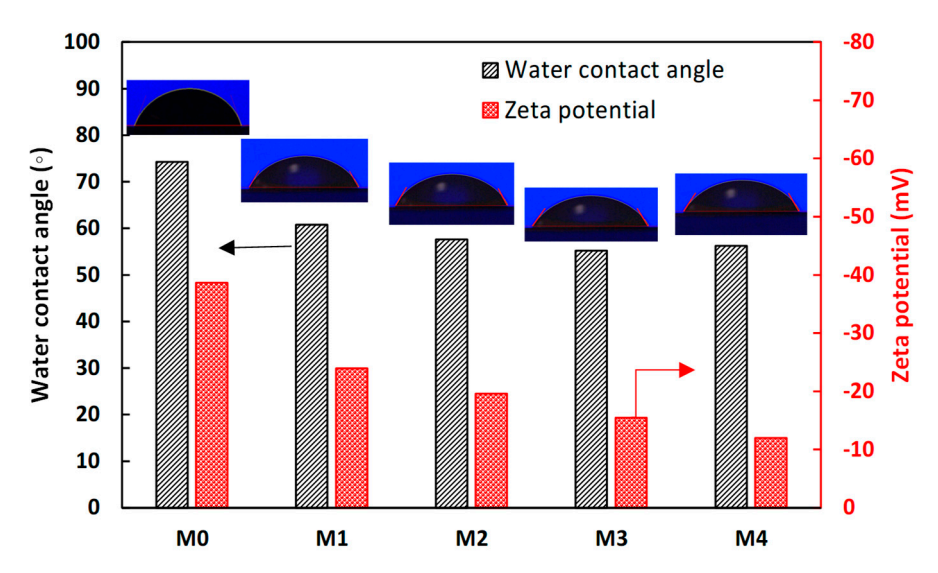


**Figure 11.** The water contact angle and Zeta potential of the tested membranes.

Surface charge can significantly affect the filtration and dye/salt separation performance of membranes [8]. The charge of the membrane surface was evaluated by measuring the zeta potential of the investigated membranes at pH 7 and a temperature of 25 °C. The results are also presented in Figure 11. The pristine PVDF membrane had a negative zeta potential of  $-38.7 \pm 2.6$  mV, which is attributed to the existence of PVDF polar molecules' inherent dipolar polarization effect on the base polymer [60]. The value of the zeta potential of the modified membranes decreased steadily with the increase in the loading of COF-TCPP (Fe) until reaching  $-12 \pm 1.4$  mV for M4. This might be due to the deposited layer of COF that covered the surface of negatively charged PVDF.

The mechanical properties of the examined membranes were evaluated using stress-strain graphs. Figure 12 shows the stress–strain curves of the pristine PVDF and COFTCPP (Fe)@ PVDF(M3) membranes. It can be seen that the tensile strength of the pristine membrane was increased from  $1.68\times10^7$  to  $1.77\times10^7$  Pa by depositing the COF-TCPP (Fe) particles, as the thickness increased after the deposition. The elastic modulus improved marginally from  $4.83\times10^8$  Pa for the pristine membrane to  $4.98\times10^8$  Pa for the COF-based membrane. The break elongation was 10.75% and 10.12% for the pristine and COF-based membranes, respectively.

#### 3.3. Performance of COF-TCPP (Fe) @ PVDF Membrane

# 3.3.1. Permeability/Selectivity Performance

The perm-selectivity performance of the pristine PVDF and the modified membranes was evaluated through a nanofiltration test. Figure 13 shows the pure water flux (PWF) and NaCl/Congo red rejection efficiency for the various investigated membranes. The pristine PVDF membrane yielded a PWF of 133.6 L  $\rm m^{-2}~h^{-1}$  bar $^{-1}$  and a Congo red rejection

Compounds **2025**, 5, 34 12 of 20

efficiency of 73.3%, with a negligible NaCl rejection efficiency of 2.4%. The PWF decreased gradually from 92.2 to 64.1 L m $^{-2}$  h $^{-1}$  bar $^{-1}$ , while the rejection efficiencies of Congo red and NaCl increased steadily from 94.8 to 99.6% and from 7.8 to 19.4%, respectively, as the loading of COF-TCPP (Fe) increased from 4 to 16 mg mL $^{-1}$ . Although the water flux was still able to penetrate through the COF layer, the increase in the thickness of the COF layer would cause more penetration resistance, consequently decreasing the water flux and increasing the rejection efficiency. The thickness of the deposited layer was proportional to the concentration of the COF-TCPP (Fe) during the vacuum filtration process, as evident in Figure 6. Considering the trade-off between permeability and selectivity, a loading concentration of 12 mg mL $^{-1}$  (M3) was chosen for further examination.

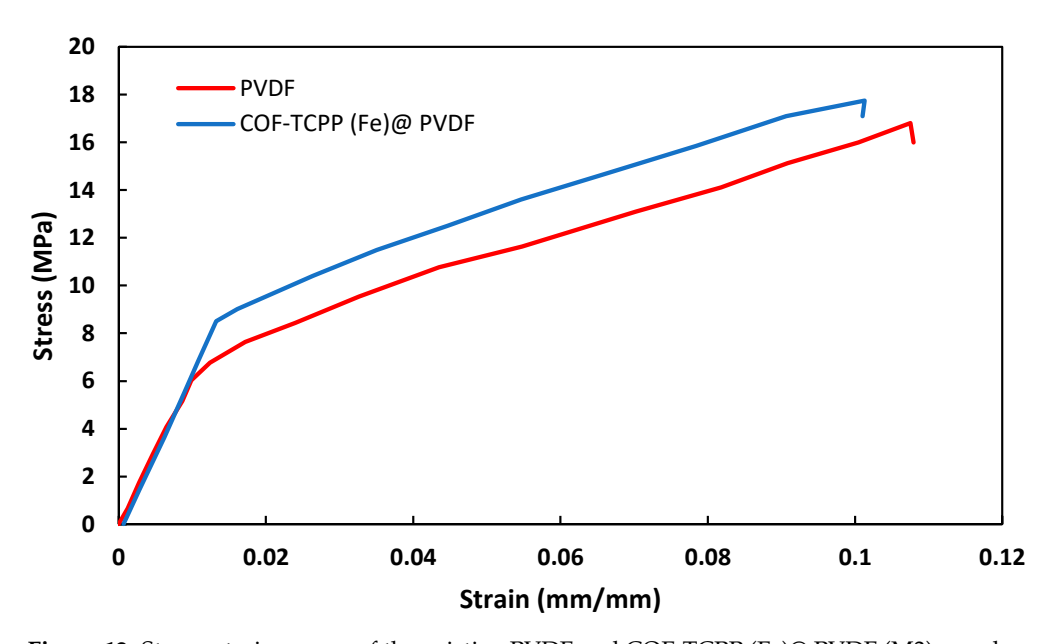


Figure 12. Stress–strain curves of the pristine PVDF and COF-TCPP (Fe)@ PVDF (M3) membranes.

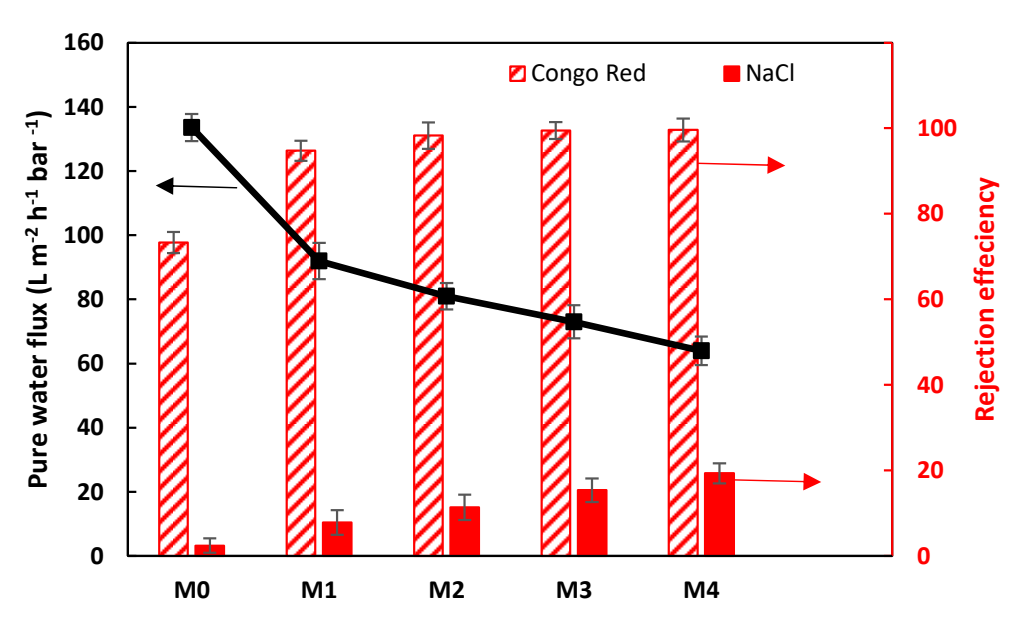


Figure 13. The water flux and Congo red/NaCl rejection efficiency of the various membranes tested.

# 3.3.2. Single Salt/Dye Separation

The sieving performance of the chosen membrane (M3) toward several salts and organic dyes was examined, and the results are illustrated in Figure 14. It can be seen that the membrane yielded salt rejection efficiencies of 29.9% (Na<sub>2</sub>SO<sub>4</sub>), 15.4% (NaCl), 7.8%

Compounds **2025**, 5, 34 13 of 20

 $(MgCl_2)$ , 9.3%  $(MgSO_4)$ , and 6.1%  $(CaCl_2)$ . Those results were 4, 6.3, 4.4, 2.9, and 2.4 times, respectively, higher than the corresponding values of the pristine membrane. However, the rejection efficiencies of M3 were relatively low due to the electrostatic attraction between the positively charged salts and the negatively charged membrane (Donnan effect) [8]. The rejection performance of bivalent salts  $(MgCl_2, MgSO_4, and CaCl_2)$  was lower than that of the monovalent salts  $(Na_2SO_4 \text{ and } NaCl)$  as the attraction force formed between bivalent ions  $(Mg^+ \text{ and } Ca^+)$  was higher than that of the monovalent ion  $(Na^+)$  [61,62].

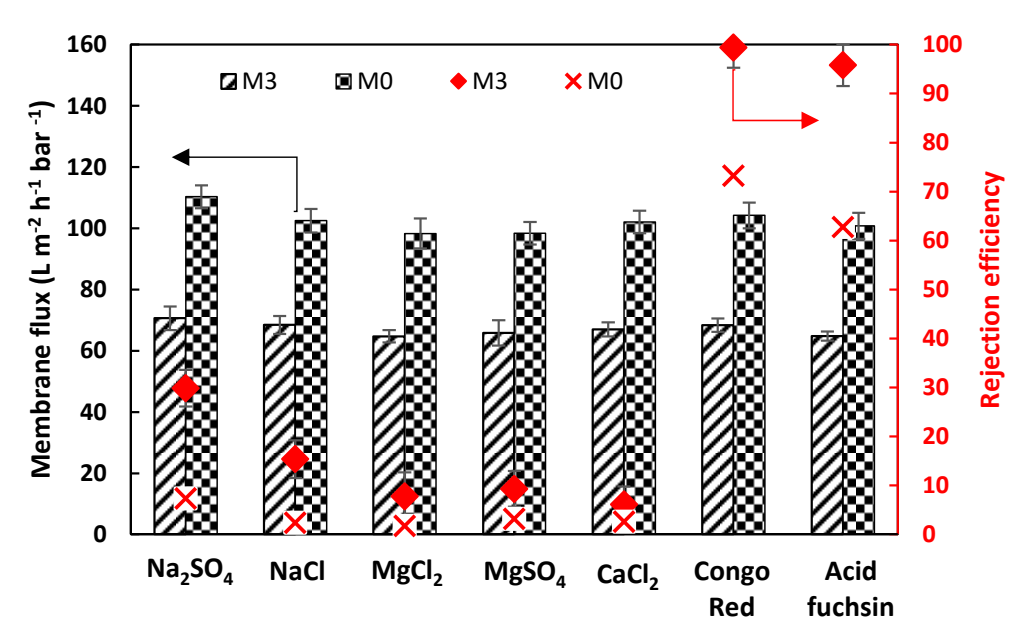


Figure 14. Membrane flux and rejection efficiency of M0 and M3 against various dyes and salts.

Two negatively charged dyes, Congo red (Mw: 696.66 Da, dimension  $\approx$  2.56 nm  $\times$  0.73 nm) and acid fuchsin (Mw: 585.54 Da, dimension  $\approx$  1.17 nm  $\times$  1.13 nm), were used to evaluate the dye rejection performance of the modified membrane (M3). The dyes were dissolved in water at a concentration of 50 ppm and used as a feed solution in the filtration test. It is evident from the color change in Figure 15 that the membrane offered high rejection efficiency against the dyes.

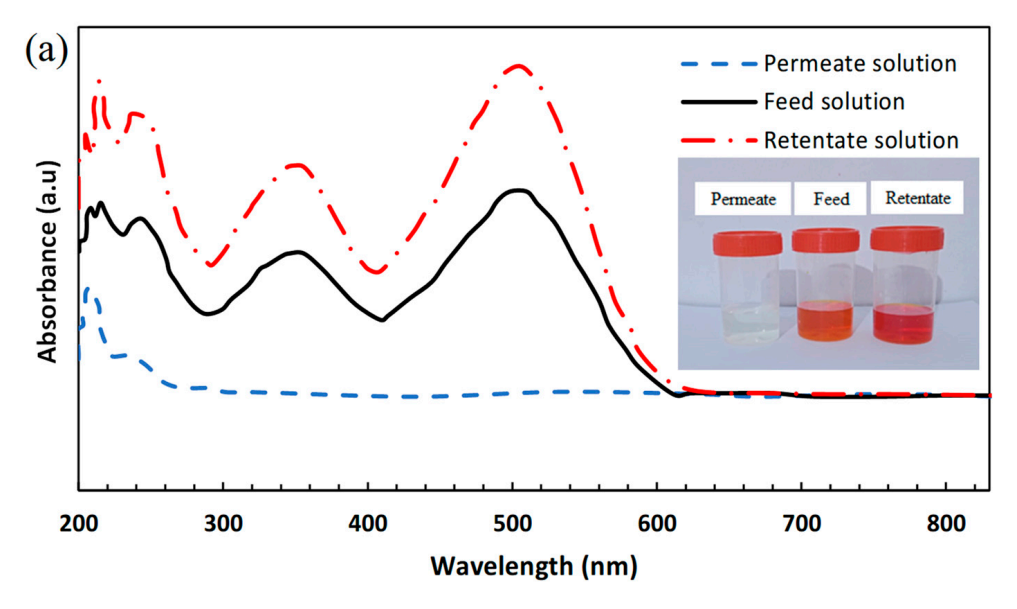
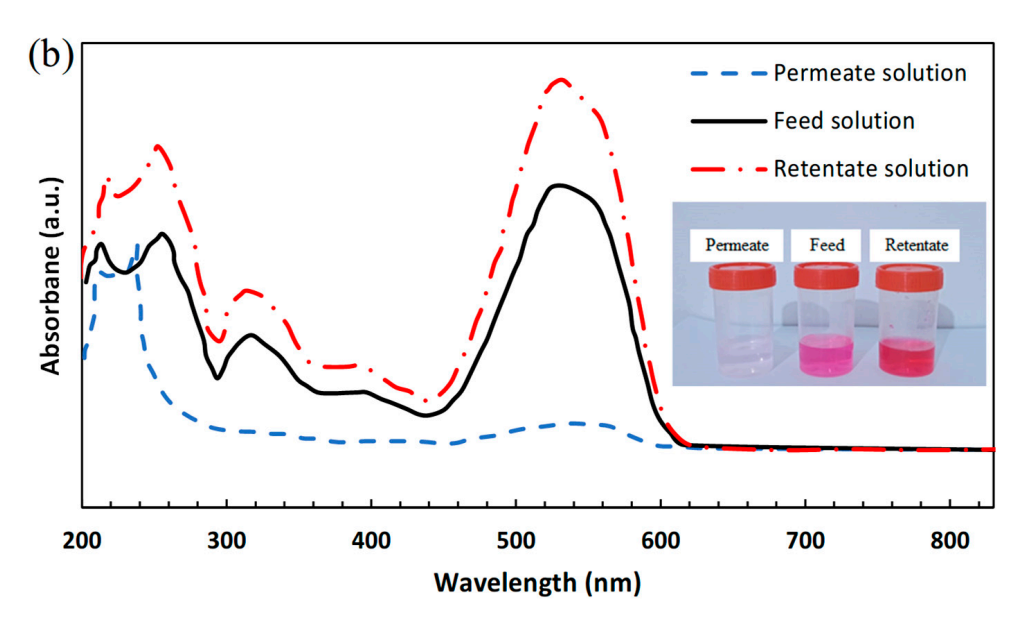


Figure 15. Cont.

Compounds **2025**, 5, 34 14 of 20



**Figure 15.** UV-vis absorption spectra of dye molecules of (a) Congo red at a feed concentration of 50 ppm and  $\lambda$  of 200–800 nm, and (b) acid fuchsin at a feed concentration of 50 ppm and  $\lambda$  of 200–800 nm.

Figure 14 also shows that the tested membrane exhibited rejection efficiencies of 99.5% (Congo red) and 95.8% (acid fuchsin). Achieving such high values of dye rejection can be explained in the context of the Donnan effect and the size-sieving mechanism, as both the membrane surface and the dyes have the same charge (negative), resulting in an electrostatic repulsive force between them. However, the Donnan effect did not significantly impact the rejection mechanism, as the rejection efficiencies of Congo red and acid fuchsin were 73.3% and 62.8%, respectively, for the negatively charged pristine PVDF membrane (Figure 11). On the other hand, the size-sieving played an essential role in the dye rejection efficiency. As explained earlier, the COF-deposited particles on the walls of the membrane pores tend to partially block the pore, making the transport mechanism mainly dependent on the molecular size of the dye. The dye rejection of the Congo red was higher than that of the acid fuchsin, as the Congo red has a molecular dimension higher than that of the acid fuchsin. It is worth mentioning that a negligible portion of dyes was absorbed by the membrane as evaluated through the mass conservation of the dyes on the three solutions (i.e., feed, permeate, and retentate).

#### 3.3.3. Salt/Dye Mixture Separation

Dyeing wastewater usually contains a considerable amount of salt. Thus, it is essential to investigate the influence of salt on the separation performance of dye/salt mixtures. A mixture of various NaCl concentrations (0.5–2.5 g/L) with a constant concentration of Congo red (0.1 g/L) was used as the feed solution in filtration. Figure 16 shows the effect of NaCl concentration on the membrane flux and rejection efficiency of the NaCl/Congo red mixture of M3. Generally, the membrane flux decreases with an increase in NaCl concentration. For instance, the membrane flux dropped from 68.1 to 59.7 L m $^{-2}$  h $^{-1}$  bar $^{-1}$  when the NaCl concentration increased from 0.5 to 2.5 g/L. This can be attributed to the increase in the concentration polarization of the NaCl ions on the surface of the membrane [63]. The Congo red rejection efficiency exhibited decreasing behavior with the salt concentration due to the presence of NaCl ions, which facilitated a more uniform dispersion of Congo red molecules in the feed solution. Consequently, the Congo red molecules of the dye/salt mixture can easily transport through the membrane [8]. On the other hand, the rejection efficiency of NaCl declined as the concentration of NaCl in the feed solution intensified.

Compounds **2025**, 5, 34 15 of 20

This is due to the increase in the concentration gradient of NaCl near the membrane surface, which increases the amount of salt transported through the membrane [64].

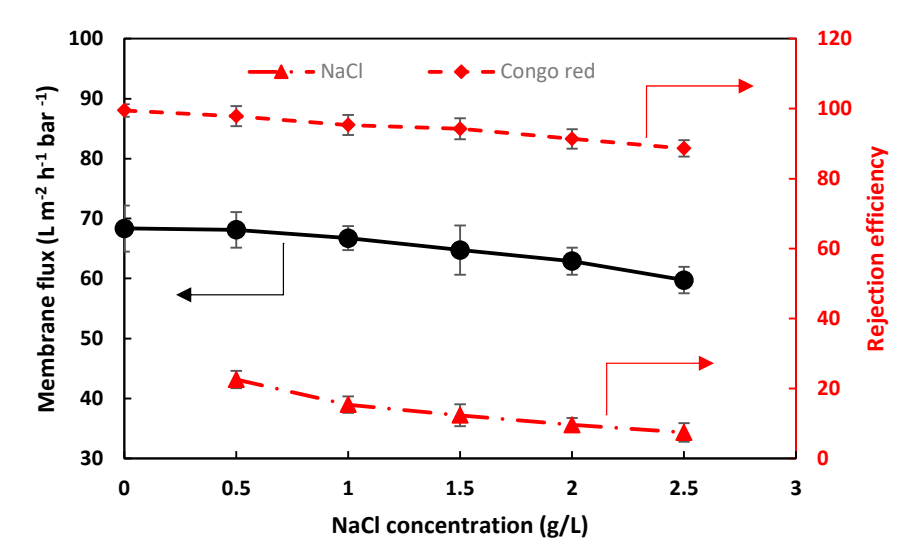


**Figure 16.** The effect of NaCl concentration on the membrane flux and NaCl/Congo red rejection efficiencies of M3.

The cyclic test was conducted to evaluate the performance of the membrane after regeneration by washing the used membrane with DI water and reusing it in the filtration test. Figure 17 shows the membrane flux and the rejection efficiency of the optimum membrane against Congo red and acid fuchsin dyes. It can be observed for both dyes that the membrane flux decreased as the regeneration cycles increased. This might be due to the penetration of the dye's molecules into the passing paths, leading them being blocked partially and causing more penetration resistance. It seems that washing with water was not enough to clear the passing paths from the penetrated molecules. For instance, the membrane flux in the Congo red experiments was  $68.34 \, \text{L m}^{-2} \, \text{h}^{-1} \, \text{bar}^{-1}$  for the first cycle and then deteriorated to  $56.92 \, \text{L m}^{-2} \, \text{h}^{-1} \, \text{bar}^{-1}$  for the fifth cycle. On the other hand, the rejection efficiency of the membrane against the dyes was also influenced negatively by the washing process. However, the rejection efficiency of Congo red after five cycles (decreasing from 99.48% to 97.68%) showed a smaller decline compared to that of acid fuchsin (from 95.82% to 86.38%). This difference can be attributed to the molecular size, as Congo red molecules are larger than those of acid fuchsin.

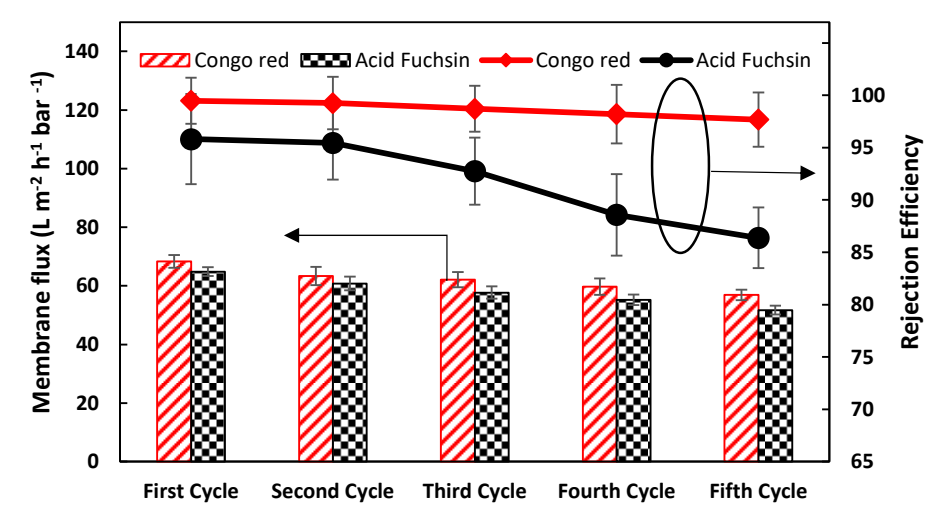


**Figure 17.** The regeneration test of M3 for the membrane flux and dye rejection efficiency of Congo red and acid fuchsin.

Compounds **2025**, 5, 34 16 of 20

To evaluate the stability of COF-TCPP (Fe) membranes, the membranes were maintained in DI water, and their appearance was assessed after a certain period. Figure 18 shows the COF-based membranes after being soaked for about 36 days. It can be observed that all the membranes demonstrated good apparent stability. There were no damages or detachment noticed, which can be attributed to the crosslinking between the NH<sub>2</sub> on the surface of the substrate and the oxygen group of COF-TCPP (Fe) [8].

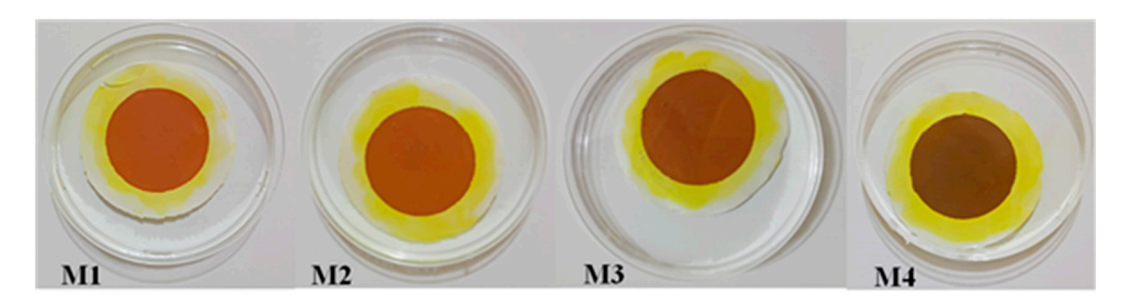


**Figure 18.** Digital photos of the apparent stability of COF-TCPP (Fe) membranes after 36 days in aqueous solution.

To highlight the performance enhancement of the proposed COF-based membrane, the results of the dye separation of the present membrane were compared to other results of reported COF-based membranes. The comparison is detailed in Table 1. In general, membranes with high Congo red rejection efficiency (over 99%) mainly offered low water flux, of about  $50 \, \text{L m}^{-2} \, \text{h}^{-1} \, \text{bar}^{-1}$ . The present COF-based membrane under optimized loading concentration possessed a membrane flux of  $68.4 \, \text{L m}^{-2} \, \text{h}^{-1} \, \text{bar}^{-1}$ , while the rejection efficiency was kept high at 99.5%.

**Table 1.** The comparison of membrane dye separation for the present membrane (M3) with other composite nanofiltration membranes.

COF	Substrate	Dye	Rejection Efficiency	Membrane Flux (L m <sup>-2</sup> h <sup>-1</sup> bar <sup>-1</sup> )	Reference
LZU1	Al <sub>2</sub> O <sub>3</sub>	Methyl blue	99.2	76	[30]
TpPa	PSF	Congo red	99.5	50	[65]
TpBd	PSF	Congo red	99.5	33.6	[66]
TpTGCL	PAN	Methylene blue	99	24	[24]
COF-300	$Al_2O_3$	Chrome black T	97.4	79	[67]
TBDH	Nylon	Congo red	99	439.4	[32]
Hz-TFPTZ	PSF/PVP	Basic blue 41	92	94.7	[33]
ТрЕВ	PAN	Congo red	99	32.3	[68]
MPD-TEB	Nylon	Congo red	98.6	94.4	[69]
Tp-TAPA	PAN	Congo red	99	68.1	[70]
Т́р-ТТА	mPSF	Chrome black T	98.1	36.5	[25]
ZIF-8	PA	Congo red	99.98	2.26	[71]
PVA	PSSNa-PSf	Congo red	99.68	7.7	[72]
TA	GOQDs-PAN	Congo red	99.8	11.7	[73]
Fe(III)-phos-(PEI)	HPAN	Acid fuchsin	98.99	5.7	[74]
LDHs	PEI-M	Acid fuchsin	97.5	19.86	[75]
PEI	PAA	Acid fuchsin	99	2	[76]
GO/NH <sub>2</sub> -Fe <sub>3</sub> O <sub>4</sub> -8	PVDF	Congo red	94	78	[8]
GO/COF-1	PAN	Congo red	99.62	31.09	[62]
GO	PAN	Congo red	98.54	6.73	[62]
DA/PEG-MXene	PVDF	Methylene Blue	94.11	70.235	[77]
COF-TCPP (Fe)	PVDF	Congo red	99.5	68.4	Present study
COF-TCPP (Fe)	PVDF	Acid fuchsin	95.8	64.8	Present study

# 4. Conclusions

In this study, a composite COF/polymeric membrane was fabricated using the vacuum-assisted interfacial polymerization method. The particles of COF-TCPP (Fe) (porphyrinic-based COF) were deposited on a PVDF substrate. Various COF loading

Compounds 2025, 5, 34 17 of 20

concentrations were implemented during the fabrication to produce membranes with different thicknesses of the selective layer. COF and membranes were characterized using different methods to ensure the synthesis of the desired chemicals. The filtration and separation performance of the pristine and modified membranes was evaluated using a dead-end filtration cell. Various salts and dyes were dissolved and implemented as the feed solution of the cell. The results revealed that the COF loading concentration in the synthesis solution plays an essential role in the perm/selectivity performance of the modified membranes. The optimum concentration was 12 mg mL $^{-1}$ . The salt rejection efficiency of the optimal modified membrane was higher by 4, 6.3, 4.4, 2.9, and 2.4 times against Na<sub>2</sub>SO<sub>4</sub>, NaCl, MgCl<sub>2</sub>, MgSO<sub>4</sub>, and CaCl<sub>2</sub>, respectively, compared to the corresponding values of the pristine membrane. The Congo red and acid fuchsin rejection efficiencies of the optimal modified membrane were higher by 35.7% and 52.6% compared to the pristine membrane. The modified membrane also demonstrated effective salt/dye separation performance. The appreciable membrane flux and improved rejection efficiency, combined with the simplicity of fabrication, can make the modified membrane a promising candidate for various applications, such as water purification and wastewater treatment. However, further investigations are recommended to optimize the performance of the proposed membrane by using different substrate membranes and/or various properties of the membrane and manipulating the porous properties of the COF, such as the specific surface area and pore size.

**Author Contributions:** Conceptualization, F.A.-G.; methodology, F.A.-G. and M.M.A.-M.; formal analysis, F.A.-G. and H.K.A.; investigation, M.M.A.-M.; resources, H.K.A.; data curation, F.A.-G., M.M.A.-M. and H.K.A.; writing—original draft preparation, F.A.-G.; writing—review and editing, F.A.-G., M.M.A.-M. and H.K.A.; visualization, M.M.A.-M.; supervision, F.A.-G. All authors have read and agreed to the published version of the manuscript.

**Funding:** This research received no external funding.

**Data Availability Statement:** The data presented in this study are available upon request from the corresponding author, as they are part of ongoing research.

**Acknowledgments:** The first author would like to thank Southern Technical University for the administrative and technical support. During the preparation of this manuscript, the authors used Grammarly to correct grammar and spelling errors.

**Conflicts of Interest:** The authors declare no conflicts of interest.

# References

- 1. Zango, Z.U.; Binzowaimil, A.M.; Aldaghri, O.A.; Eisa, M.H.; Garba, A.; Ahmed, N.M.; Lim, J.W.; Ng, H.-S.; Daud, H.; Jumbri, K.; et al. Applications of covalent organic frameworks for the elimination of dyes from wastewater: A state-of-the-arts review. *Chemosphere* 2023, 343, 140223. [CrossRef]
- 2. Altaf, A.; Baig, N.; Sohail, M.; Sher, M.; Ul-Hamid, A.; Altaf, M. Covalent organic frameworks: Advances in synthesis and applications. *Mater. Today Commun.* **2021**, *28*, 102612. [CrossRef]
- 3. Bagheri, A.R.; Aramesh, N.; Sher, F.; Bilal, M. Covalent organic frameworks as robust materials for mitigation of environmental pollutants. *Chemosphere* **2021**, *270*, 129523. [CrossRef] [PubMed]
- 4. Ding, X.; Nie, M.; Cheng, S.; Li, R.; Wang, Y.; Ali, A.S.; Han, X.; Sun, Y. Voltage-Gated Pillararene-Intercalated MXene membranes for adjusting water purification. *Sep. Purif. Technol.* **2025**, *365*, 132667. [CrossRef]
- 5. Zhang, Q.; Ni, C.; Deng, N.; Huang, X. Tailoring Electronic and Morphology Features of Iron-Doped Ni2P Nanoflowers for Enhanced Ammonia Electrosynthesis in Solid Electrolyte Reactors. *Adv. Energy Mater.* **2025**, *15*, 2405442. [CrossRef]
- 6. Rasheed, T. Covalent organic frameworks as promising adsorbent paradigm for environmental pollutants from aqueous matrices: Perspective and challenges. *Sci. Total Environ.* **2022**, *833*, 155279. [CrossRef]
- 7. Abdellah, A.R.; Abdelhamid, H.N.; El-Adasy, A.-B.A.A.M.; Atalla, A.A.; Aly, K.I. One-pot synthesis of hierarchical porous covalent organic frameworks and two-dimensional nanomaterials for selective removal of anionic dyes. *J. Environ. Chem. Eng.* **2020**, *8*, 104054. [CrossRef]

Compounds **2025**, 5, 34 18 of 20

8. Dong, L.; Li, M.; Zhang, S.; Si, X.; Bai, Y.; Zhang, C. NH<sub>2</sub>-Fe<sub>3</sub>O<sub>4</sub>-regulated graphene oxide membranes with well-defined laminar nanochannels for desalination of dye solutions. *Desalination* **2020**, *476*, 114227. [CrossRef]

- 9. Solayman, H.M.; Hossen, M.A.; Abd Aziz, A.; Yahya, N.Y.; Leong, K.H.; Sim, L.C.; Monir, M.U.; Zoh, K.-D. Performance evaluation of dye wastewater treatment technologies: A review. *J. Environ. Chem. Eng.* **2023**, *11*, 109610. [CrossRef]
- 10. Sukhatskiy, Y.; Shepida, M.; Sozanskyi, M.; Znak, Z.; Gogate, P.R. Periodate-based advanced oxidation processes for wastewater treatment: A review. *Sep. Purif. Technol.* **2023**, 304, 122305. [CrossRef]
- 11. Guo, S.; Wan, Y.; Chen, X.; Luo, J. Loose nanofiltration membrane custom-tailored for resource recovery. *Chem. Eng. J.* **2021**, 409, 127376. [CrossRef]
- 12. Lin, J.; Ye, W.; Zeng, H.; Yang, H.; Shen, J.; Darvishmanesh, S.; Luis, P.; Sotto, A.; Van der Bruggen, B. Fractionation of direct dyes and salts in aqueous solution using loose nanofiltration membranes. *J. Membr. Sci.* **2015**, 477, 183–193. [CrossRef]
- 13. Du, C.; Li, P.; Zhuang, Z.; Fang, Z.; He, S.; Feng, L.; Chen, W. Highly porous nanostructures: Rational fabrication and promising application in energy electrocatalysis. *Coord. Chem. Rev.* **2022**, *466*, 214604. [CrossRef]
- 14. Albdoor, A.K.; Ma, Z.; Cooper, P.; Al-Ghazzawi, F.; Liu, J.; Richardson, C.; Wagner, P. Air-to-air enthalpy exchangers: Membrane modification using metal-organic frameworks, characterisation and performance assessment. *J. Clean. Prod.* **2021**, 293, 126157. [CrossRef]
- 15. Al-Ghazzawi, F.; Conte, L.; Potts, M.W.; Richardson, C.; Wagner, P. Reactive Extrusion Printing of Zeolitic Imidazolate Framework Films. *ACS Appl. Mater. Interfaces* **2024**, *16*, 44270–44277. [CrossRef] [PubMed]
- 16. Wang, L.; Li, X.; Yang, B.; Xiao, K.; Duan, H.; Zhao, H. The chemical stability of metal-organic frameworks in water treatments: Fundamentals, effect of water matrix and judging methods. *Chem. Eng. J.* **2022**, *450*, 138215. [CrossRef]
- 17. Kumar, R.; Zhang, C.; Itta, A.K.; Koros, W.J. Highly permeable carbon molecular sieve membranes for efficient CO<sub>2</sub>/N<sub>2</sub> separation at ambient and subambient temperatures. *J. Membr. Sci.* **2019**, *583*, 9–15. [CrossRef]
- 18. Zuluaga, S.; Fuentes-Fernandez, E.M.; Tan, K.; Xu, F.; Li, J.; Chabal, Y.J.; Thonhauser, T. Understanding and controlling water stability of MOF-74. *J. Mater. Chem. A* **2016**, *4*, 5176–5183. [CrossRef]
- 19. Zhivulin, V.E.; Trofimov, E.A.; Zaitseva, O.V.; Sherstyuk, D.P.; Cherkasova, N.A.; Taskaev, S.V.; Vinnik, D.A.; Alekhina, Y.A.; Perov, N.S.; Naidu, K.C. Preparation, phase stability, and magnetization behavior of high entropy hexaferrites. *iScience* **2023**, *26*, 107077. [CrossRef]
- 20. Trukhanov, S.; Trukhanov, A.; Panina, L.; Kostishyn, V.; Turchenko, V.; Trukhanova, E.; Trukhanov, A.V.; Zubar, T.; Ivanov, V.; Tishkevich, D. Temperature evolution of the structure parameters and exchange interactions in BaFe<sub>12-x</sub>In<sub>x</sub>O<sub>19</sub>. *J. Magn. Magn. Mater.* **2018**, 466, 393–405. [CrossRef]
- 21. Trukhanov, S.; Trukhanov, A.; Kostishyn, V.; Zabeivorota, N.; Panina, L.; Trukhanov, A.V.; Turchenko, V.; Trukhanova, E.; Oleynik, V.; Yakovenko, O. High-frequency absorption properties of gallium weakly doped barium hexaferrites. *Philos. Mag.* **2019**, 99, 585–605. [CrossRef]
- 22. Wang, J.; Zhuang, S. Covalent organic frameworks (COFs) for environmental applications. *Coord. Chem. Rev.* **2019**, *400*, 213046. [CrossRef]
- 23. Zhu, R.; Zhang, P.; Zhang, X.; Yang, M.; Zhao, R.; Liu, W.; Li, Z. Fabrication of synergistic sites on an oxygen-rich covalent organic framework for efficient removal of Cd (II) and Pb (II) from water. *J. Hazard. Mater.* 2022, 424, 127301. [CrossRef]
- 24. Sheng, F.; Li, X.; Li, Y.; Afsar, N.U.; Zhao, Z.; Ge, L.; Xu, T. Cationic covalent organic framework membranes for efficient dye/salt separation. *J. Membr. Sci.* **2022**, *644*, 120118. [CrossRef]
- 25. Zhang, Y.; Ye, H.; Chen, D.; Li, N.; Xu, Q.; Li, H.; He, J.; Lu, J. In situ assembly of a covalent organic framework composite membrane for dye separation. *J. Membr. Sci.* **2021**, *628*, 119216. [CrossRef]
- 26. Miao, Q.; Wang, Y.; Chen, D.; Cao, N.; Pang, J. Development of novel ionic covalent organic frameworks composite nanofiltration membranes for dye/salt separation. *J. Hazard. Mater.* **2024**, *465*, 133049. [CrossRef]
- 27. Dai, J.-Y.; Fang, Y.-X.; Xu, Z.-L.; Pandaya, D.; Liang, J.; Yan, H.-F.; Tang, Y.-J. Robust covalent organic frameworks membranes for ultrafast dye/salt separation in harsh environments. *Desalination* **2023**, *568*, 117025. [CrossRef]
- 28. Alduraiei, F.; Kumar, S.; Liu, J.; Nunes, S.P.; Szekely, G. Rapid fabrication of fluorinated covalent organic polymer membranes for organic solvent nanofiltration. *J. Membr. Sci.* **2022**, *648*, 120345. [CrossRef]
- 29. Wang, G.; Chen, Y.; Pan, C.; Chen, H.; Ding, S.; Chen, X. Rapid synthesis of self-standing covalent organic frameworks membrane via polyethylene glycol-assisted space-confined strategy. *J. Membr. Sci.* **2022**, *652*, 120494. [CrossRef]
- 30. Fan, H.; Gu, J.; Meng, H.; Knebel, A.; Caro, J. High-flux membranes based on the covalent organic framework COF-LZU1 for selective dye separation by nanofiltration. *Angew. Chem. Int. Ed.* **2018**, *57*, 4083–4087. [CrossRef]
- 31. Zhang, Y.; Guo, J.; Han, G.; Bai, Y.; Ge, Q.; Ma, J.; Lau, C.H.; Shao, L. Molecularly soldered covalent organic frameworks for ultrafast precision sieving. *Sci. Adv.* **2021**, *7*, eabe8706. [CrossRef]
- He, Y.; Lin, X. Fabricating compact covalent organic framework membranes with superior performance in dye separation. J. Membr. Sci. 2021, 637, 119667. [CrossRef]

Compounds 2025, 5, 34 19 of 20

33. Mokhtari, N.; Dinari, M.; Fashandi, H. Developing polysulfone-based mixed matrix membrane containing hydrazone-linked covalent organic frameworks towards dye wastewater purification. *Chem. Eng. J.* **2022**, *446*, 137456. [CrossRef]

- 34. Wang, R.; Shi, X.; Zhang, Z.; Xiao, A.; Sun, S.-P.; Cui, Z.; Wang, Y. Unidirectional diffusion synthesis of covalent organic frameworks (COFs) on polymeric substrates for dye separation. *J. Membr. Sci.* **2019**, *586*, 274–280. [CrossRef]
- Kandambeth, S.; Biswal, B.P.; Chaudhari, H.D.; Rout, K.C.; Mitra, S.; Karak, S.; Das, A.; Mukherjee, R.; Kharul, U.K.; Banerjee, R. Selective molecular sieving in self-standing porous covalent-organic-framework membranes. *Adv. Mater.* 2017, 29, 1603945. [CrossRef]
- 36. Khan, N.A.; Zhang, R.; Wu, H.; Shen, J.; Yuan, J.; Fan, C.; Cao, L.; Olson, M.A.; Jiang, Z. Solid–vapor interface engineered covalent organic framework membranes for molecular separation. *J. Am. Chem. Soc.* **2020**, *142*, 13450–13458. [CrossRef]
- 37. Wang, H.; Wang, M.; Liang, X.; Yuan, J.; Yang, H.; Wang, S.; Ren, Y.; Wu, H.; Pan, F.; Jiang, Z. Organic molecular sieve membranes for chemical separations. *Chem. Soc. Rev.* **2021**, *50*, 5468–5516. [CrossRef]
- 38. He, G.; Zhang, R.; Jiang, Z. Engineering covalent organic framework membranes. Acc. Mater. Res. 2021, 2, 630-643. [CrossRef]
- 39. Kong, F.-X.; Yue, L.; Yang, Z.; Sun, G.; Chen, J.-F. Cross-linked covalent organic framework-based membranes with trimesoyl chloride for enhanced desalination. *ACS Appl. Mater. Interfaces* **2021**, *13*, 21379–21389. [CrossRef]
- 40. Zhang, C.; Li, Y.; Rao, J.; Lin, X.; Huang, Y.; He, Y. Congo red stitched covalent organic framework membrane for dye separation. *Sep. Purif. Technol.* **2025**, *354*, 129021. [CrossRef]
- 41. Li, X.; Qiao, J.; Chee, S.W.; Xu, H.-S.; Zhao, X.; Choi, H.S.; Yu, W.; Quek, S.Y.; Mirsaidov, U.; Loh, K.P. Rapid, Scalable Construction of Highly Crystalline Acylhydrazone Two-Dimensional Covalent Organic Frameworks via Dipole-Induced Antiparallel Stacking. *J. Am. Chem. Soc.* 2020, 142, 4932–4943. [CrossRef]
- 42. Li, X.; Xu, H.-S.; Leng, K.; Chee, S.W.; Zhao, X.; Jain, N.; Xu, H.; Qiao, J.; Gao, Q.; Park, I.-H.; et al. Partitioning the interlayer space of covalent organic frameworks by embedding pseudorotaxanes in their backbones. *Nat. Chem.* 2020, 12, 1115–1122. [CrossRef] [PubMed]
- 43. Cheng, S.-Q.; Liu, Y.; Sun, Y. Macrocycle-based metal–organic and covalent organic framework membranes. *Coord. Chem. Rev.* **2025**, *534*, 216559. [CrossRef]
- 44. Zhang, X.; Tu, B.; Cao, Z.; Fang, M.; Zhang, G.; Yang, J.; Ying, Y.; Sun, Z.; Hou, J.; Fang, Q. Anomalous mechanical and electrical interplay in a covalent organic framework monolayer membrane. *J. Am. Chem. Soc.* **2023**, *145*, 17786–17794. [CrossRef]
- 45. Hussain, S.; Peng, X. Ultra-fast photothermal-responsive Fe-TCPP-based thin-film nanocomposite membranes for ON/OFF switchable nanofiltration. *Sep. Purif. Technol.* **2021**, 278, 119528. [CrossRef]
- 46. Albdoor, A.K.; Ma, Z.; Cooper, P. Moisture diffusion measurement and evaluation for porous membranes used in enthalpy exchangers. *Energy Procedia* **2019**, *160*, 499–506. [CrossRef]
- 47. Zhao, X.; Yuan, L.; Zhang, Z.-Q.; Wang, Y.-S.; Yu, Q.; Li, J. Synthetic Methodology for the Fabrication of Porous Porphyrin Materials with Metal–Organic–Polymer Aerogels. *Inorg. Chem.* **2016**, *55*, 5287–5296. [CrossRef] [PubMed]
- 48. Lovo de Carvalho, A.; Ferreira, B.F.; Martins, C.H.G.; Nassar, E.J.; Nakagaki, S.; Machado, G.S.; Rives, V.; Trujillano, R.; Vicente, M.A.; Gil, A.; et al. Tetracarboxyphenylporphyrin–Kaolinite Hybrid Materials as Efficient Catalysts and Antibacterial Agents. *J. Phys. Chem. C* 2014, 118, 24562–24574. [CrossRef]
- 49. Liao, H.; Wang, H.; Ding, H.; Meng, X.; Xu, H.; Wang, B.; Ai, X.; Wang, C. A 2D porous porphyrin-based covalent organic framework for sulfur storage in lithium–sulfur batteries. *J. Mater. Chem. A* 2016, 4, 7416–7421. [CrossRef]
- 50. Mahajan, P.G.; Dige, N.C.; Vanjare, B.D.; Phull, A.R.; Kim, S.J.; Hong, S.-K.; Lee, K.H. Synthesis, Photophysical Properties and Application of New Porphyrin Derivatives for Use in Photodynamic Therapy and Cell Imaging. *J. Fluoresc.* **2018**, 28, 871–882. [CrossRef]
- 51. Fang, Y.; Zhu, C.-Y.; Yang, H.-C.; Zhang, C.; Xu, Z.-K. Polyamide nanofiltration membranes by vacuum-assisted interfacial polymerization: Broad universality of Substrate, wide window of monomer concentration and high reproducibility of performance. *J. Colloid Interface Sci.* **2024**, 655, 327–334. [CrossRef]
- 52. Liu, S.; Kang, L.; Hu, J.; Jung, E.; Zhang, J.; Jun, S.C.; Yamauchi, Y. Unlocking the Potential of Oxygen-Deficient Copper-Doped Co3O4 Nanocrystals Confined in Carbon as an Advanced Electrode for Flexible Solid-State Supercapacitors. *ACS Energy Lett.* **2021**, *6*, 3011–3019. [CrossRef]
- Kandambeth, S.; Shinde, D.B.; Panda, M.K.; Lukose, B.; Heine, T.; Banerjee, R. Enhancement of Chemical Stability and Crystallinity in Porphyrin-Containing Covalent Organic Frameworks by Intramolecular Hydrogen Bonds. *Angew. Chem. Int. Ed.* 2013, 52, 13052–13056. [CrossRef]
- 54. Xu, C.; Yang, Z.; Zhang, S.; Gao, X.; Bao, L.; Meng, Z. Porphyrin-based covalent organic frameworks with synergistic active centers for enhanced peroxidase-like activity as a colorimetric biosensing platform. *Microchem. J.* **2025**, 210, 112918. [CrossRef]
- 55. Zhang, Y.; Ma, J.; Wang, D.; Xu, C.; Sheng, S.; Cheng, J.; Bao, C.; Li, Y.; Tian, H. Fe-TCPP@CS nanoparticles as photodynamic and photothermal agents for efficient antimicrobial therapy. *Biomater. Sci.* **2020**, *8*, 6526–6532. [CrossRef] [PubMed]
- 56. Pan, X.; Huang, X.; Deng, N. Short-Chain Carboxylic Acids Influencing Mineralization Mechanisms of Ferrihydrite Transformation to Hematite and Goethite. *Environ. Sci. Technol.* **2025**, *59*, 12910–12919. [CrossRef]

Compounds **2025**, 5, 34 20 of 20

57. Huang, G.; Su, T.-M.; Zeng, K.; Guo, Y.-A.; Zhao, S.-K.; Wei, S.-J. Mesoporous chitosan-immobilized iron tetrakis(4-carboxyphenyl)porphyrin as a model of cytochrome P-450 enzyme for oxidation of ethylbenzene. *Appl. Organomet. Chem.* **2018**, *32*, e4140. [CrossRef]

- 58. Shan, Z.; Sun, Y.; Wu, M.; Zhou, Y.; Wang, J.; Chen, S.; Wang, R.; Zhang, G. Metal-porphyrin-based three-dimensional covalent organic frameworks for electrocatalytic nitrogen reduction. *Appl. Catal. B Environ.* **2024**, 342, 123418. [CrossRef]
- 59. Zhang, M.; Zheng, R.; Ma, Y.; Chen, R.; Sun, X.; Sun, X. A novel one-dimensional porphyrin-based covalent organic framework. *Molecules* **2019**, 24, 3361. [CrossRef]
- 60. Li, X.; Chen, Y.; Hu, X.; Zhang, Y.; Hu, L. Desalination of dye solution utilizing PVA/PVDF hollow fiber composite membrane modified with TiO<sub>2</sub> nanoparticles. *J. Membr. Sci.* **2014**, *471*, 118–129. [CrossRef]
- 61. Zhu, J.; Tian, M.; Hou, J.; Wang, J.; Lin, J.; Zhang, Y.; Liu, J.; Van der Bruggen, B. Surface zwitterionic functionalized graphene oxide for a novel loose nanofiltration membrane. *J. Mater. Chem. A* **2016**, *4*, 1980–1990. [CrossRef]
- 62. Zhang, X.; Li, H.; Wang, J.; Peng, D.; Liu, J.; Zhang, Y. In-situ grown covalent organic framework nanosheets on graphene for membrane-based dye/salt separation. *J. Membr. Sci.* **2019**, *581*, 321–330. [CrossRef]
- 63. Wang, L.; Zhao, L.; Xiao, X.; Wang, X.; Cao, J.; Ye, H.; Li, H.; Zhang, Y. Two-dimensional Cu-FeTCPP nanozyme incorporated loose nanofiltration membrane with self-cleaning property for dye/salt separation. *Sep. Purif. Technol.* **2025**, *359*, 130551. [CrossRef]
- 64. Wei, X.; Kong, X.; Sun, C.; Chen, J. Characterization and application of a thin-film composite nanofiltration hollow fiber membrane for dye desalination and concentration. *Chem. Eng. J.* **2013**, 223, 172–182. [CrossRef]
- 65. Wang, R.; Shi, X.; Xiao, A.; Zhou, W.; Wang, Y. Interfacial polymerization of covalent organic frameworks (COFs) on polymeric substrates for molecular separations. *J. Membr. Sci.* **2018**, *566*, 197–204. [CrossRef]
- 66. Wang, T.; Wu, H.; Zhao, S.; Zhang, W.; Tahir, M.; Wang, Z.; Wang, J. Interfacial polymerized and pore-variable covalent organic framework composite membrane for dye separation. *Chem. Eng. J.* **2020**, *384*, 123347. [CrossRef]
- 67. Wang, Z.; Si, Z.; Cai, D.; Shufeng Li, G.L.; Qin, P. Synthesis of stable COF-300 nanofiltration membrane via in-situ growth with ultrahigh flux for selective dye separation. *J. Membr. Sci.* **2020**, *615*, 118466. [CrossRef]
- 68. Basel, N.; Liu, Q.; Fan, L.; Wang, Q.; Xu, N.; Wan, Y.; Dong, Q.; Huang, Z.; Guo, T. Surface charge enhanced synthesis of TpEB-based covalent organic framework (COF) membrane for dye separation with three typical charge properties. *Sep. Purif. Technol.* 2022, 303, 122243. [CrossRef]
- 69. Fang, Y.-X.; Lin, Y.-F.; Xu, Z.-L.; Mo, J.-W.; Li, P.-P. A novel clover-like COFs membrane fabricated via one-step interfacial polymerization for dye/salt separation. *J. Membr. Sci.* **2023**, *673*, 121470. [CrossRef]
- 70. Zhao, S.; Di, N.; Lei, R.; Wang, J.; Wang, Z. Triphenylamine-based COFs composite membrane fabricated through oligomer-triggered interfacial polymerization. *J. Membr. Sci.* **2023**, *672*, 121424. [CrossRef]
- 71. Wang, L.; Fang, M.; Liu, J.; He, J.; Deng, L.; Li, J.; Lei, J. The influence of dispersed phases on polyamide/ZIF-8 nanofiltration membranes for dye removal from water. *RSC Adv.* **2015**, *5*, 50942–50954. [CrossRef]
- 72. Liu, M.; Zhou, C.; Dong, B.; Wu, Z.; Wang, L.; Yu, S.; Gao, C. Enhancing the permselectivity of thin-film composite poly (vinyl alcohol)(PVA) nanofiltration membrane by incorporating poly (sodium-p-styrene-sulfonate)(PSSNa). *J. Membr. Sci.* **2014**, 463, 173–182. [CrossRef]
- 73. Zhang, C.; Wei, K.; Zhang, W.; Bai, Y.; Sun, Y.; Gu, J. Graphene oxide quantum dots incorporated into a thin film nanocomposite membrane with high flux and antifouling properties for low-pressure nanofiltration. *ACS Appl. Mater. Interfaces* **2017**, *9*, 11082–11094. [CrossRef] [PubMed]
- 74. Li, P.; Wang, Z.; Yang, L.; Zhao, S.; Song, P.; Khan, B. A novel loose-NF membrane based on the phosphorylation and cross-linking of polyethyleneimine layer on porous PAN UF membranes. *J. Membr. Sci.* **2018**, *555*, 56–68. [CrossRef]
- 75. Zhao, S.; Zhu, H.; Wang, Z.; Song, P.; Ban, M.; Song, X. A loose hybrid nanofiltration membrane fabricated via chelating-assisted in-situ growth of Co/Ni LDHs for dye wastewater treatment. *Chem. Eng. J.* **2018**, 353, 460–471. [CrossRef]
- 76. Tang, H.; Ji, S.; Gong, L.; Guo, H.; Zhang, G. Tubular ceramic-based multilayer separation membranes using spray layer-by-layer assembly. *Polym. Chem.* **2013**, *4*, 5621–5628. [CrossRef]
- 77. Mu, M.; Graham, N.; Yu, W.; Sun, K.; Xu, X.; Liu, T. Optimal cross-linking of MXene-based membranes for high rejection and low adsorption with long-term stability for water treatment. *J. Membr. Sci.* **2024**, 701, 122738. [CrossRef]

**Disclaimer/Publisher's Note:** The statements, opinions and data contained in all publications are solely those of the individual author(s) and contributor(s) and not of MDPI and/or the editor(s). MDPI and/or the editor(s) disclaim responsibility for any injury to people or property resulting from any ideas, methods, instructions or products referred to in the content.